METHOD

Open Access

PseudotimeDE: inference of differential gene expression along cell pseudotime with well-calibrated *p*-values from single-cell RNA sequencing data

Dongyuan Song[1] and Jingyi Jessica Li[2,3,4,5*]

*Correspondence: jli@stat.ucla.edu;
lijy03@g.ucla.edu
[2]Department of Statistics, University
of California, Los Angeles, CA
90095-1554, USA
[3]Department of Human Genetics,
University of California, Los Angeles,
CA 90095-7088, USA
Full list of author information is
available at the end of the article

Abstract

To investigate molecular mechanisms underlying cell state changes, a crucial analysis is to identify differentially expressed (DE) genes along the pseudotime inferred from single-cell RNA-sequencing data. However, existing methods do not account for pseudotime inference uncertainty, and they have either ill-posed *p*-values or restrictive models. Here we propose PseudotimeDE, a DE gene identification method that adapts to various pseudotime inference methods, accounts for pseudotime inference uncertainty, and outputs well-calibrated *p*-values. Comprehensive simulations and real-data applications verify that PseudotimeDE outperforms existing methods in false discovery rate control and power.

Introduction

In recent years, single-cell RNA-sequencing (scRNA-seq) technologies have undergone rapid development to dissect transcriptomic heterogeneity and to discover cell types or states in complex tissues [1, 2]. Embracing the capacity to measure transcriptomes of numerous cells simultaneously, scRNA-seq provides a powerful means to capture continuous cell-state transition across cells, and it has been used to study key cellular processes such as immune response [3] and cell development [4]. For example, a study of human fibroblasts identified distinct fibroblast subtypes responsible for mediating inflammation or tissue damage in arthritis [5]; a study of maternal-fetal interface tissue revealed new cell states and the importance of this tissue in maternal immune tolerance of paternal antigens [6]; a study of thymic development elucidated new principles of naïve T cell repertoire formation [7].

Pseudotime inference, also known as trajectory inference, is one of the most thriving scRNA-seq data analysis topics. The concept of "pseudotime" was first proposed in 2014

[8], and since then, more than 40 pseudotime inference methods have been developed [9]. Pseudotime inference aims to infer the ordering of cells along a lineage based on the cells' gene expression profiles measured by scRNA-seq, and the inferential target is "pseudotime," a time-like variable indicating the relative position a cell takes in a lineage. By establishing a temporal dimension in a static scRNA-seq dataset, pseudotime inference allows the probing of individual genes' expression dynamics along with continuous cell-state changes. If a gene's mean expression changes along pseudotime, the gene is referred to as differentially expressed (DE) and is likely to play an important role in the underlying cellular process that gives rise to the pseudotime. Identifying DE genes is the most crucial analysis after pseudotime inference because genes are the most fundamental functional units for understanding biological mechanisms.

Several methods have been developed to identify DE genes along inferred cell pseudotime. Popular pseudotime inference methods—TSCAN [10], Slingshot [11], Monocle [8], and Monocle2 [12]—include a built-in functionality for identifying DE genes after pseudotime inference. Their common approach is to use the generalized additive model (GAM) [13–15] to fit each gene's expression level in a cell as a smooth-curve function of the cell's inferred pseudotime. However, these built-in methods for DE gene identification are restricted as an add-on and downstream step of the pseudotime inference method in the same software package, and they cannot take external, user-provided pseudotime as input. Therefore, if users would like to use a new pseudotime inference method, they cannot use these built-in DE methods.

To our knowledge, only two DE gene identification methods can take any user-provided pseudotime. The first and state-of-the-art one is tradeSeq, which uses the negative binomial generalized additive model (NB-GAM) to model the relationship between each gene's expression in a cell and the cell's pseudotime [16]. Its p-value calculation is based on a chi-squared distribution, an inaccurate approximation to the null distribution. As a result, its p-values lack the correct probability interpretation. This issue is noted in the tradeSeq paper: "Rather than attaching strong probabilistic interpretations to the p-values (which, as in most RNA-seq applications, would involve a variety of hard-to-verify assumptions and would not necessarily add much value to the analysis), we view the p-values simply as useful numerical summaries for ranking the genes for further inspection." Hence, the uncalibrated p-values of tradeSeq cannot be used for p-value-based statistical procedures such as the type I error control and the false discovery rate (FDR) control. The second method is Monocle3, better known as a pseudotime inference method [17], yet it also allows DE gene identification based on user-provided cell covariates via regression analysis. For clarity, we refer to the pseudotime inference and differential expression functionalities in Monocle3 as "Monocle3-PI" and "Monocle3-DE," respectively. (Note that by "Monocle3-DE," we mean the "regression analysis `fit_models()`," not the "graph-autocorrelation analysis `graph_test()`," in the Monocle3 R package; only the former works for user-provided pseudotime.) Monocle3-DE uses the generalized linear model (GLM) to identify DE genes for a user-provided covariate, e.g., pseudotime. However, GLM is more restrictive than GAM in that GLM assumes the logarithmic transformation of a gene's expected read count in a cell is a strictly linear function of the cell's pseudotime, while this assumption does not hold for many genes [18]. Hence, Monocle3-DE would miss those complex relationships between gene expression and pseudotime that do not satisfy its GLM assumption. In

other words, Monocle3-DE's restrictive GLM assumption impairs its power in identifying DE genes.

Besides the scRNA-seq methods we mentioned above, there are methods developed for identifying physical-time-varying DE genes from bulk RNA-seq time-course data. Among those methods, the ones allowing for continuous time can in principle be used to identify DE genes along pseudotime. Two examples of such methods are NBAMSeq [19] and ImpulseDE2 [20]. NBAMSeq is similar to tradeSeq in the use of NB-GAM, but it uses the Bayesian shrinkage method in DESeq2 [21] to estimate gene variances, while tradeSeq does not. ImpulseDE2 [20], a method favorably rated in a benchmark study for bulk RNA-seq data [22], models gene differential expression by a unique "impulse" model. A later study modified ImpulseDE2 to identify DE genes along pseudotime from scRNA-seq data [16]. However, the performance of NBAM-Seq and ImpulseDE2 on scRNA-seq data lacks benchmarking. Loosely related, many methods can identify DE genes between discrete cell clusters, groups, or conditions [23–27]; however, these methods are inapplicable to finding DE genes along continuous pseudotime.
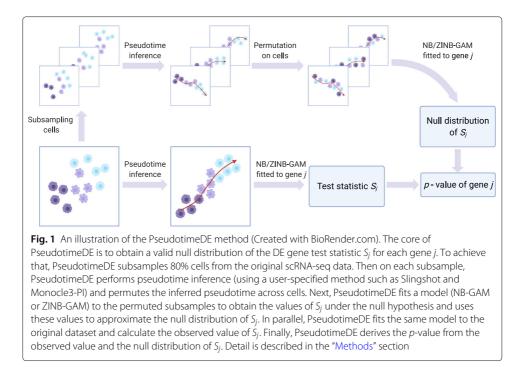
More importantly, the existing methods that identify DE genes along pseudotime have a common limitation: they ignore the uncertainty of inferred cell pseudotime, which they consider as one fixed value per cell. This issue arises from the fact that most pseudotime inference methods only return point estimates of cell pseudotime without uncertainty quantification (i.e., every cell only receives an inferred pseudotime without a standard error), with few exceptions [28, 29]. Hence, downstream DE gene identification methods treat these point estimates as fixed and ignore their uncertainty. However, this ignorance of uncertainty would result in invalid p-values, leading to either failed FDR control or power loss. This critical problem has been noted in several pseudotime inference method papers [10, 11, 28] and in the tradeSeq paper [16], yet it remains an open challenge to our knowledge.

Motivated by the ill-posed p-value issue of existing pseudotime-based differential expression methods, we propose PseudotimeDE, the first method that accommodates user-provided pseudotime inference methods, takes into account the random nature of inferred pseudotime, and outputs well-calibrated p-values. PseudotimeDE uses subsampling to estimate pseudotime inference uncertainty and propagates the uncertainty to its statistical test for DE gene identification. As the most notable advantage of PseudotimeDE over existing methods, PseudotimeDE's well-calibrated p-values ensures the reliability of FDR control and other downstream analyses, as well as avoiding unnecessary power loss due to overly-conservative p-values.

Results

Overview of the PseudotimeDE method

The statistical method of PseudotimeDE consists of four major steps: subsampling, pseudotime inference, model fitting, and hypothesis testing (Fig. 1). The first two steps are performed at the cell level and include all informative genes (whose selection depends on the pseudotime inference method, e.g., Slingshot and Monocle3-PI), while the last two steps are performed on every gene that is potentially DE.

Fig. 1 An illustration of the PseudotimeDE method (Created with BioRender.com). The core of PseudotimeDE is to obtain a valid null distribution of the DE gene test statistic S_j for each gene j. To achieve that, PseudotimeDE subsamples 80% cells from the original scRNA-seq data. Then on each subsample, PseudotimeDE performs pseudotime inference (using a user-specified method such as Slingshot and Monocle3-PI) and permutes the inferred pseudotime across cells. Next, PseudotimeDE fits a model (NB-GAM or ZINB-GAM) to the permuted subsamples to obtain the values of S_j under the null hypothesis and uses these values to approximate the null distribution of S_j. In parallel, PseudotimeDE fits the same model to the original dataset and calculate the observed value of S_j. Finally, PseudotimeDE derives the p-value from the observed value and the null distribution of S_j. Detail is described in the "Methods" section

1 In the subsampling step, PseudotimeDE subsamples 80% of cells from the original dataset to capture the uncertainty of pseudotime inference, the same technique as used in [9, 11, 30].

2 In the pseudotime inference step, PseudotimeDE applies a user-specified pseudotime inference method to the original dataset and each subsample, so that every cell receives its inferred pseudotime in the original dataset and all the subsamples that include it. To construct null cases where genes are non-DE for later hypothesis testing, PseudotimeDE permutes the inferred pseudotime in each subsample, independent of other subsamples.

3 In the model fitting step, PseudotimeDE fits NB-GAM or zero-inflated negative binomial GAM (ZINB-GAM) to every gene in the original dataset to obtain a test statistic that indicates the effect size of the inferred pseudotime on the gene's expression.

4 In the hypothesis testing step, for every gene, Pseudotime fits the same model used for the original dataset to the permuted subsamples to obtain approximate null values of the gene's test statistic (the null values are approximate because the subsamples do not have the same number of cells as in the original dataset). To save the number of subsamples needed and to improve the p-value resolution, Pseudotime fits a Gamma distribution or a mixture of two Gamma distributions to these null values. It subsequently uses the fitted parametric distribution as the approximate null distribution of the test statistic. Finally, PseudotimeDE calculates a right-tail p-value for the gene from the gene's test statistic in the original dataset and the approximate null distribution.

Further detail of PseudotimeDE is described in the "Methods" section.

Simulations verify that PseudotimeDE outperforms existing methods in the validity of *p*-values and the identification power

We use a widely-used simulator `dyntoy` [9, 16] to generate four synthetic scRNA-seq datasets, among which three are single-lineage datasets with low-, medium-, and high-dispersion levels, and the other is a bifurcation dataset. Since the single-lineage high-dispersion dataset best resembles the real scRNA-seq data (Additional file 1: Fig. S1), we use it as our primary case. We apply two pseudotime inference methods—Slingshot and Monocle3-PI—to each synthetic dataset to infer cell pseudotime.

First, we find that PseudotimeDE successfully captures the underlying uncertainty of inferred pseudotime. The first layer—"linear uncertainty"—reflects the randomness of inferred cell pseudotime within a cell lineage (Fig. 2a, & c). Figure 2b, & d shows the distributions of individual cells' inferred pseudotime by Slingshot and Monocle3-PI, respectively, across 1000 subsampled datasets, confirming that linear uncertainty is specific to pseudotime inference methods. Between the two methods, Monocle3-PI demonstrates greater linear uncertainty. The second layer—"topology uncertainty"—reflects the randomness of lineage construction. The synthetic bifurcation dataset contains two cell lineages. Slingshot correctly constructs the bifurcation topology from the original dataset and the 1000 subsampled datasets. While Monocle3-PI captures the bifurcation topology from the original dataset (Fig. 2e), it fails to capture the topology from over 50%
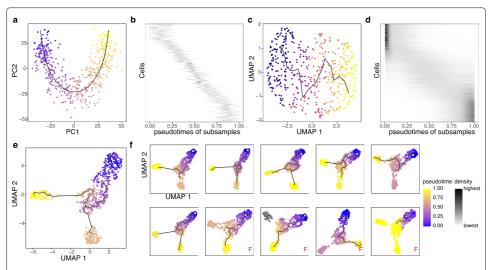

Fig. 2 PseudotimeDE captures the uncertainty in pseudotime inference. **a** Visualization of synthetic single-lineage cells marked with inferred pseudotime by Slingshot (using PCA). The black curve denotes the inferred lineage. **b** The distributions of individual cells' inferred pseudotime by Slingshot across subsamples. In the vertical axis, cells are ordered by their true time in the lineage used in simulation; for every cell (a vertical coordinate), black dots have horizontal coordinates corresponding to the cell's inferred pseudotime in the subsamples that include the cell. The more horizontally spread out the black dots, the greater uncertainty the pseudotime inference has. **c** Visualization of synthetic single-lineage cells marked with inferred pseudotime by Monocle3-PI (using UMAP). The black curve denotes the inferred lineage. Compared with (a), the inferred lineage is more wiggling. **d** The distributions of individual cells' inferred pseudotime by Monocle3-PI across subsamples. Compared with (**b**), the uncertainty in pseudotime inference is greater. **e** Visualization of synthetic bifurcating cells marked with inferred pseudotime by Monocle3-PI (using UMAP). Monocle3-PI recovers the bifurcation topology. **f** Visualization of ten subsamples of the cells in (**e**), marked with inferred pseudotime by Monocle3-PI (using UMAP) on each subsample. Four out of the ten subsamples do not have the bifurcation topology correctly inferred (labeled with red "F"), revealing the uncertainty in pseudotime inference by Monocle3-PI. In panels **a**, **c**, **e**, and **f**, inferred pseudotime is represented by a color scale from 0 (the earliest pseudotime) to 1 (the latest pseudotime)
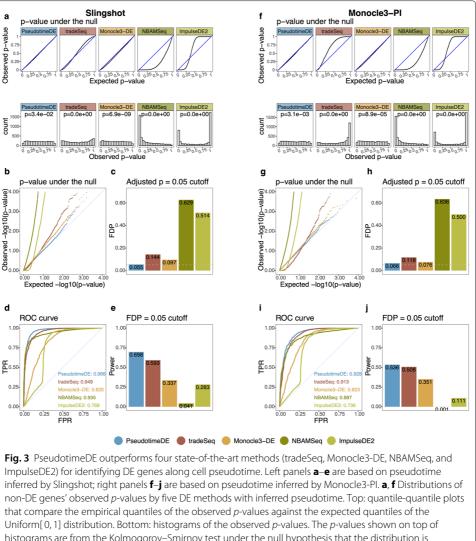
of subsamples (Fig. 2f shows randomly picked 10 subsamples), demonstrating its greater topology uncertainty than Slingshot's.

After confirming pseudotime inference uncertainty, we benchmark PseudotimeDE against four DE gene identification methods: tradeSeq, Monocle3-DE, NBAMSeq, and ImpulseDE2. The first two methods, tradeSeq and Monocle3-DE, are the state-of-the-art for scRNA-seq data analysis and thus serve as the main competitors of PseudotimeDE. In our benchmark, we first evaluate these methods in terms of the validity of their p-values, which should be uniformly distributed between 0 and 1 under the null hypothesis (i.e., a gene is not DE). Our results show that, among the five methods, PseudotimeDE generates the best-calibrated p-values that follow the expected uniform distribution most closely (Fig. 3a, & f and Additional file 1: Figs. S3–S5a & f). Among the existing four methods, only Monocle3-DE provides roughly calibrated p-values, while tradeSeq, NBAMSeq, and ImpulseDE2 output p-values that are much deviated from the expected uniform distribution. This observation is confirmed by the Kolmogorov–Smirnov test, which evaluates how closely p-values follow the uniform distribution. Since the identification of DE genes relies on a small p-value cutoff, the smaller p-values are more important than the larger ones. Hence, we re-plot the p-values on $-\log_{10}$ scale to closely examine the calibration of small p-values (Fig. 3b, & g and Additional file 1: Figs. S3–S5b & g). Again, PseudotimeDE returns the best-calibrated p-values, while the other four methods generate overly small p-values that would inflate false discoveries. This is reflected in our results: at a target 5% FDR threshold, PseudotimeDE leads to the best FDR control among all methods (Fig. 3c, & h and Additional file 1: Figs. S3–S5c & h).

Next, we compare these methods in terms of their ability to distinguish DE genes from non-DE genes, ability measured by the area under the receiver operating characteristic curve (AUROC) values (Fig. 3d, & i and Additional file 1: Figs. S3–S5d & i). Pseudo-timeDE achieves the highest AUROC values. Among the other four methods, tradeSeq and NBAMSeq have slightly lower AUROC values than PseudotimeDE's, and Monocle3-DE and ImpulseDE2 have much lower AUROC values than the other three methods'. The reason is that PseudotimeDE, tradeSeq, and NBAMSeq all use the flexible model NB-GAM, while Monocle3-DE and ImpulseDE2 use much more restrictive models, which limit their power.

Realizing that the ill-calibrated p-values of the existing four methods invalidate their FDR control, we compare all five methods in terms of their power under an actual 5% false discovery proportion (FDP, defined as the proportion of false discoveries among the discoveries in one synthetic dataset) instead of the nominal 5% FDR. Our results show that PseudotimeDE achieves the highest power on all datasets except for the bifurcation dataset, where PseudotimeDE has slightly lower power than tradeSeq's (Fig. 3e, & j and Additional file 1: Figs. S3–S5e & j). These results demonstrate the high power of PseudotimeDE and its effective FDR control, which is lacking in existing methods.

In summary, our simulation results verify that PseudotimeDE outperforms existing methods in terms of generating well-calibrated p-values, which are essential for FDR control, and identifying DE genes with high power. Notably, the two bulk RNA-seq methods, NBAMSeq and ImpulseDE2, yield worse results than the three scRNA-seq methods do. Hence, we only focus on the scRNA-seq methods in the following three real data applications.

Fig. 3 PseudotimeDE outperforms four state-of-the-art methods (tradeSeq, Monocle3-DE, NBAMSeq, and ImpulseDE2) for identifying DE genes along cell pseudotime. Left panels **a**–**e** are based on pseudotime inferred by Slingshot; right panels **f**–**j** are based on pseudotime inferred by Monocle3-PI. **a**, **f** Distributions of non-DE genes' observed p-values by five DE methods with inferred pseudotime. Top: quantile-quantile plots that compare the empirical quantiles of the observed p-values against the expected quantiles of the Uniform[0, 1] distribution. Bottom: histograms of the observed p-values. The p-values shown on top of histograms are from the Kolmogorov–Smirnov test under the null hypothesis that the distribution is Uniform[0, 1]. The larger the p-value, the more uniform the distribution is. Among the five DE methods, PseudotimeDE's observed p-values follow most closely the expected Uniform[0, 1] distribution. **b**, **g** Quantile-quantile plots of the same p-values as in **a** and **f** on the negative $\log_{10}$ scale. PseudotimeDE returns better-calibrated small p-values than the other four methods do. **c**, **h** FDPs of the five DE methods with the target FDR 0.05 (BH adjusted-$p \leq 0.05$). PseudotimeDE yields the FDP closest to 0.05. **d**, **i** ROC curves and AUROC values of the five DE methods. PseudotimeDE achieves the highest AUROC. **e**, **j** Power of the five DE methods under the FDP = 0.05 cutoff. PseudotimeDE achieves the highest power

Real data example 1: dendritic cells stimulated with lipopolysaccharide

In the first application, we compare PseudotimeDE with tradeSeq and Monocle3-DE on a dataset of mouse dendritic cells (DCs) after stimulation with lipopolysaccharide (LPS, a component of gram-negative bacteria) [31]. In this dataset, gene expression changes are expected to be associated with the immune response process. We first apply Slingshot and Monocle3-PI to this dataset to infer cell pseudotime, and then, we input the inferred pseudotime into PseudotimeDE, tradeSeq, and Monocle3-DE for DE gene identification. Consistent with our simulation results, the p-values of tradeSeq are ill-calibrated: their bimodal distributions indicate that they do not follow the uniform distribution under the null hypothesis; instead, many of them are inflated, and this inflation would lead

to power loss in DE gene identification (Fig. 4a, & e). Indeed, at a nominal Benjamini-Hochberg (BH) adjusted p-value ≤ 0.01 threshold (which corresponds to controlling the FDR $\leq 1\%$ when p-values are valid), tradeSeq identifies the smallest number of DE genes, while PseudotimeDE identifies the most DE genes, followed by Monocle3-DE. Notably, most of the DE genes identified by tradeSeq are also identified by PseudotimeDE (Fig. 4b, & f), a result consistent with the over-conservativeness of tradeSeq due to its inflated p-values. Unlike tradeSeq, Monocle3-DE does not exhibit the inflated p-value issue; however, it uses a more restrictive model than PseudotimeDE and tradeSeq do. Hence, we use functional analyses to investigate whether Monocle3-DE misses certain DE genes due to its restrictive modeling. We also investigate whether the additional DE genes found by PseudotimeDE but missed by tradeSeq or Monocle3-DE are biologically meaningful.

Our first strategy is to perform gene ontology (GO) analysis on the DE genes identified by each method and compare the enriched GO terms. We find that more GO terms are enriched (with enrichment p-values < 0.01) in the DE genes identified by PseudotimeDE (Additional file 1: Fig. S6a & c) and that the PseudotimeDE-specific GO terms are related
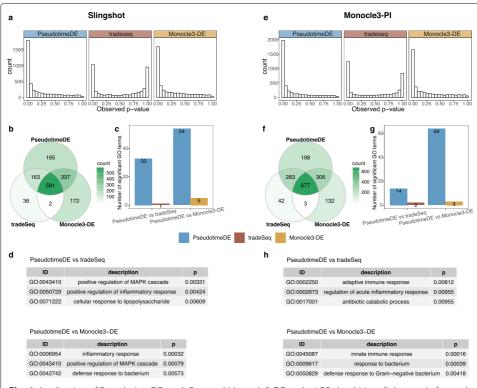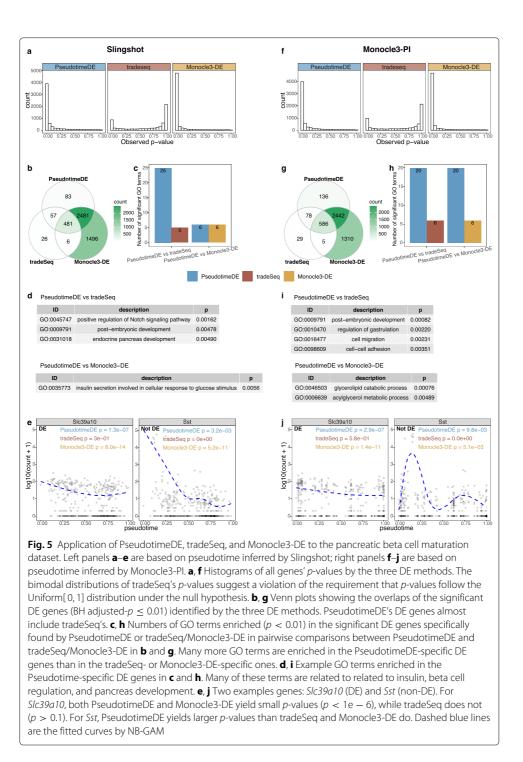

Fig. 4 Application of PseudotimeDE, tradeSeq, and Monocle3-DE to the LPS-dendritic cell dataset. Left panels **a–d** are based on pseudotime inferred by Slingshot; right panels **e–h** are based on pseudotime inferred by Monocle3-PI. **a**, **e** Histograms of all genes' p-values by the three DE methods. The bimodal distributions of tradeSeq's p-values suggest a violation of the requirement that p-values follow the Uniform[0, 1] distribution under the null hypothesis. **b**, **f** Venn plots showing the overlaps of the significant DE genes (BH adjusted-$p \leq 0.01$) identified by the three DE methods. PseudotimeDE's DE genes almost include tradeSeq's. **c**, **g** Numbers of GO terms enriched ($p < 0.01$) in the significant DE genes specifically found by PseudotimeDE or tradeSeq/Monocle3-DE in pairwise comparisons between PseudotimeDE and tradeSeq/Monocle3-DE in **b** and **f**. Many more GO terms are enriched in the PseudotimeDE-specific DE genes than in the tradeSeq- or Monocle3-DE-specific ones. **d**, **h** Example GO terms enriched in the Pseudotime-specific DE genes in **c** and **g**. Many of these terms are related to LPS, immune process, and defense to bacterium

to immune responses (Additional file 1: Fig. S6b & d). However, comparing enriched GO terms does not directly reflect the difference of DE genes identified by different methods. Hence, our second strategy is to probe the functions of the DE genes that are uniquely identified by one method in pairwise comparisons of PseudotimeDE vs. tradeSeq and PseudotimeDE vs. Monocle3-DE. We first perform GO analysis on each set of uniquely identified DE genes. For a fair comparison of two methods, we remove the overlapping DE genes found by both methods from the background gene list in GO analysis. Our results show that many more GO terms are enriched (with enrichment p-values < 0.01) in Pseudotime-specific DE genes than in tradeSeq- or Monocle3-DE-specific DE genes (Fig. 4c, & g). Moreover, many of those PseudotimeDE-specific GO terms are directly related to the immune responses of DCs to LPS stimulation, including the GO terms "cellular response to lipopolysaccharide" and "defense response to Gram-negative bacterium" (Fig. 4d, & h; Additional file 2: Table S1). To focus more on immune responses, we next perform enrichment analysis using the immunologic signatures (C7) in the Molecular Signatures Database (MSigDB) [32]. Our results show that only PseudotimeDE-specific DE genes have enriched MSigDB C7 terms (with BH adjusted p-values < 0.01), while tradeSeq- and Monocle3-DE-specific DE genes have almost no enrichment (Additional file 1: Fig. S7a & c). More importantly, many enriched terms in PseudotimeDE-specific DE genes were found by previous studies of DCs stimulated with LPS (see examples in Additional file 1: Fig. S7b & d; Additional file 2: Table S1); this is direct evidence that supports the validity of PseudotimeDE-specific DE genes. For illustration purpose, we visualize the expression levels of some known and novel DE genes identified by PseudotimeDE using UMAP, and clear DE patterns are observed (Additional file 1: Fig. S8–S9). In conclusion, our functional analyses verify that PseudotimeDE identifies biologically meaningful DE genes missed by tradeSeq and Monocle3-DE, confirming that PseudotimeDE has high power in addition to its well-calibrated p-values.

Real data example 2: pancreatic beta cell maturation

In the second application, we compare PseudotimeDE with tradeSeq and Monocle3-DE on a dataset of mouse beta cell maturation process [33]. We first apply Slingshot and Monocle3-PI to this dataset to infer cell pseudotime, and then, we input the inferred pseudotime into PseudotimeDE, tradeSeq, and Monocle3-DE for DE gene identification. Consistent with previous results, the p-values of tradeSeq follow a bimodal distribution, suggesting that many of them are incorrectly inflated (Fig. 5a, & f). At the nominal BH-adjusted p-value ≤ 0.01 level, PseudotimeDE identifies the second most DE genes, fewer than Monocle3-DE's identified DE genes and much more than tradeSeq's (Fig. 5b, & g). As the numbers of identified DE genes cannot reflect these methods' performance, we use three approaches to evaluate the DE genes identified by each method.

  We first perform GO analysis on each set of uniquely identified DE genes, using the same pairwise comparisons of PseudotimeDE vs. tradeSeq and PseudotimeDE vs. Monocle3-DE as for the LPS-dendritic data. Our results show that more GO terms are enriched (with enrichment p-values < 0.01) in PseudotimeDE-specific DE genes than in tradeSeq- or Monocle3-DE-specific DE genes (Fig. 5c, & h). Moreover, many of those PseudotimeDE-specific GO terms are directly related to pancreatic beta cell development, e.g., "positive/negative regulation of Notch signaling pathway" [34] and "endocrine pancreas development" (Fig. 5c, & h; Additional file 3: Table S2). As a complementary

Fig. 5 Application of PseudotimeDE, tradeSeq, and Monocle3-DE to the pancreatic beta cell maturation dataset. Left panels **a**–**e** are based on pseudotime inferred by Slingshot; right panels **f**–**j** are based on pseudotime inferred by Monocle3-PI. **a**, **f** Histograms of all genes' *p*-values by the three DE methods. The bimodal distributions of tradeSeq's *p*-values suggest a violation of the requirement that *p*-values follow the Uniform[0, 1] distribution under the null hypothesis. **b**, **g** Venn plots showing the overlaps of the significant DE genes (BH adjusted-$p \leq 0.01$) identified by the three DE methods. PseudotimeDE's DE genes almost include tradeSeq's. **c**, **h** Numbers of GO terms enriched ($p < 0.01$) in the significant DE genes specifically found by PseudotimeDE or tradeSeq/Monocle3-DE in pairwise comparisons between PseudotimeDE and tradeSeq/Monocle3-DE in **b** and **g**. Many more GO terms are enriched in the PseudotimeDE-specific DE genes than in the tradeSeq- or Monocle3-DE-specific ones. **d**, **i** Example GO terms enriched in the Pseudotime-specific DE genes in **c** and **h**. Many of these terms are related to related to insulin, beta cell regulation, and pancreas development. **e**, **j** Two examples genes: *Slc39a10* (DE) and *Sst* (non-DE). For *Slc39a10*, both PseudotimeDE and Monocle3-DE yield small *p*-values ($p < 1e-6$), while tradeSeq does not ($p > 0.1$). For *Sst*, PseudotimeDE yields larger *p*-values than tradeSeq and Monocle3-DE do. Dashed blue lines are the fitted curves by NB-GAM

result, we also perform GO analysis on the DE genes identified by each method. We find that the GO terms, which are only enriched in the DE genes identified by PseudotimeDE, are related to beta cell development and thus more biologically meaningful than the GO terms that are only enriched in the DE genes identified by tradeSeq or Monocle3-DE (Additional file 1: Fig. S10b & d).

Second, we utilize the DE genes identified from bulk RNA-seq data in the original paper [33] to evaluate the DE gene rankings established by PseudotimeDE, tradeSeq, and Monocle3-DE from scRNA-seq data. Taking the bulk DE genes as a gene set, we perform the gene-set enrichment analysis (GSEA) [32] on all genes' $-\log_{10} p$-values output by PseudotimeDE, tradeSeq, and Monocle3-DE. Among the three methods, PseudotimeDE leads to the highest normalized enrichment score (NES) (Additional file 3: Table S2), suggesting that the bulk DE genes are most enriched in the top-ranked DE genes found by PseudotimeDE.
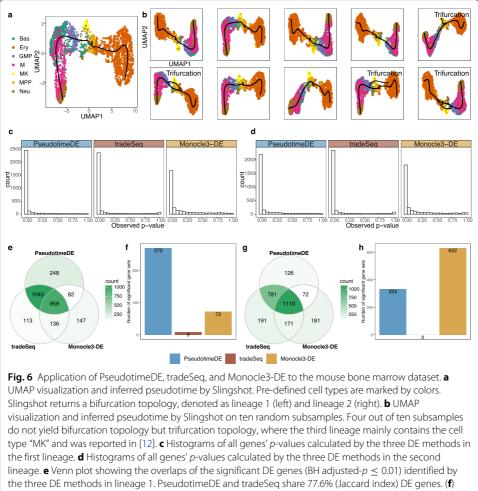
Third, we examine a highly credible DE gene *Slc39a10* [33, 35] and a verified non-DE gene *Sst* [33] as representative examples. For *Slc39a10*, both PseudotimeDE and Monocle3-DE yield small p-values ($< 10^{-6}$), while tradeSeq outputs a p-value > 0.1 and thus misses it (Fig. 5e, & g). For *Sst*, PseudotimeDE yields the largest p-value (> 0.001), while tradeSeq and Monocle3-DE yield extremely small p-values ($< 10^{-10}$) and thus mistaken it as a DE gene. Hence, PseudotimeDE has the best performance on these two representative genes.

For illustration purpose, we visualize the expression levels of some known and novel DE genes identified by PseudotimeDE using UMAP, and clear DE patterns are observed (Additional file 1: Figs. S11–S12).

Real data example 3: bone marrow differentiation

In the third application, we compare PseudotimeDE with tradeSeq and Monocle3-DE on a dataset of mouse bone marrow differentiation [36]. We apply Slingshot with UMAP for dimensionality reduction to infer cell pseudotime as described in the tradeSeq paper [16]. Slingshot constructs the reported bifurcation topology (in the tradeSeq paper) on the original dataset (Fig. 6a), but it infers trifurcation topology, instead of bifurcation topology, on 40% of subsamples (Fig. 6b shows randomly picked ten subsamples). Note that the third lineage consisting of the cell type megakaryocyte (MK) was reported in the Monocle2 paper ([12]), suggesting the observed topology uncertainty may be biologically meaningful.

For a fair comparison, we only make PseudotimeDE use the subsamples with bifurcation topology inferred, because both tradeSeq and Monocle3-DE use the inferred bifurcation topology from the original data to identify DE genes. Consistent with previous results, the tradeSeq p-values follow a bimodal distribution that is unexpected for well-calibrated p-values. At a nominal BH-adjusted p-value ≤ 0.01 threshold, the three methods identify highly similar DE genes (Fig. 6e, & g). For instance, PseudotimeDE and tradeSeq share about 80% of their identified DE genes (Jaccard index). From the few method-specific DE genes, functional analyses cannot indicate which method performs better. Therefore, we use GSEA instead to evaluate methods' p-values. Surprisingly, although the three methods identify highly similar DE genes, their p-values lead to vastly different GSEA results. At the $q < 0.25$ level, PseudotimeDE and Monocle3-DE yield hundreds of enriched gene sets, while tradeSeq only yields a few or no enriched gene sets (Fig. 6f, & h; Additional file 4: Table S3). This result indicates that, besides the ranking of p-values, the nominal values of p-values are also crucial for downstream analysis such as GSEA. Hence, the well-calibrated p-values make PseudotimeDE superior to existing methods for DE gene identification and downstream analyses.
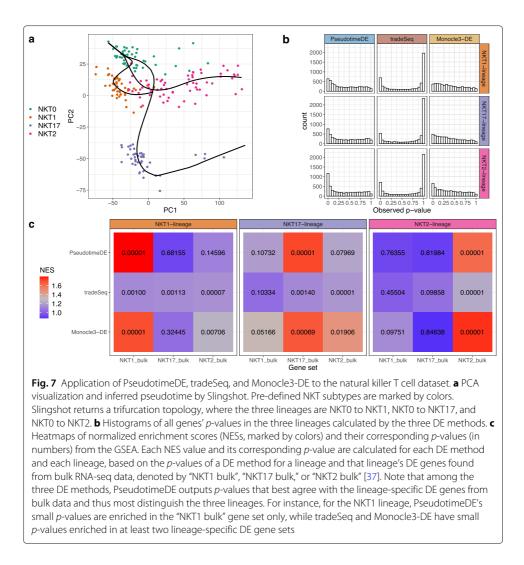
Fig. 6 Application of PseudotimeDE, tradeSeq, and Monocle3-DE to the mouse bone marrow dataset. **a** UMAP visualization and inferred pseudotime by Slingshot. Pre-defined cell types are marked by colors. Slingshot returns a bifurcation topology, denoted as lineage 1 (left) and lineage 2 (right). **b** UMAP visualization and inferred pseudotime by Slingshot on ten random subsamples. Four out of ten subsamples do not yield bifurcation topology but trifurcation topology, where the third lineage mainly contains the cell type "MK" and was reported in [12]. **c** Histograms of all genes' *p*-values calculated by the three DE methods in the first lineage. **d** Histograms of all genes' *p*-values calculated by the three DE methods in the second lineage. **e** Venn plot showing the overlaps of the significant DE genes (BH adjusted-$p \leq 0.01$) identified by the three DE methods in lineage 1. PseudotimeDE and tradeSeq share 77.6% (Jaccard index) DE genes. (**f**) Numbers of enriched gene sets ($q < 0.25$) by GSEA using the *p*-values in lineage 1 by the three DE methods. Although the DE genes are similar in **e**, PseudotimeDE yields 270 enriched gene sets, while tradeSeq only yields 9. **g** Venn plot showing the overlaps of the significant DE genes (BH adjusted-$p \leq 0.01$) identified by the three DE methods in lineage 2. Similar to lineage 1 in **g**, PseudotimeDE and tradeSeq share 77.2% (Jaccard index) DE genes. **h** Numbers of enriched gene sets ($q < 0.25$) by GSEA using the *p*-values in lineage 2 by the three DE methods. PseudotimeDE and Monocle3-DE yield hundreds of enriched gene sets, while tradeSeq does not yield any enriched gene sets

Real data example 4: natural killer T cell subtypes

In the fourth application, we compare PseudotimeDE with tradeSeq and Monocle3-DE on a dataset of natural killer T cell (NKT cell) subtypes [37]. We apply Slingshot with PCA for dimensionality reduction to infer cell pseudotime and construct the trifurcation topology (Fig. 7a) reported in the original study. We apply the three DE methods to identify DE genes in each of the three lineages. Consistent with the previous results, the *p*-values of tradeSeq follow a bimodal distribution, suggesting that many of them are incorrectly inflated (Fig. 7b).

For validation purpose, we utilize the lineage-specific DE genes identified from bulk RNA-seq data in the original study [37] to evaluate the DE gene rankings established by PseudotimeDE, tradeSeq, and Monocle3-DE from scRNA-seq data. Specifically, we perform the GSEA using the bulk DE gene sets in the same way as for the pancreatic beta cell

Fig. 7 Application of PseudotimeDE, tradeSeq, and Monocle3-DE to the natural killer T cell dataset. **a** PCA visualization and inferred pseudotime by Slingshot. Pre-defined NKT subtypes are marked by colors. Slingshot returns a trifurcation topology, where the three lineages are NKT0 to NKT1, NKT0 to NKT17, and NKT0 to NKT2. **b** Histograms of all genes' *p*-values in the three lineages calculated by the three DE methods. **c** Heatmaps of normalized enrichment scores (NESs, marked by colors) and their corresponding *p*-values (in numbers) from the GSEA. Each NES value and its corresponding *p*-value are calculated for each DE method and each lineage, based on the *p*-values of a DE method for a lineage and that lineage's DE genes found from bulk RNA-seq data, denoted by "NKT1 bulk", "NKT17 bulk," or "NKT2 bulk" [37]. Note that among the three DE methods, PseudotimeDE outputs *p*-values that best agree with the lineage-specific DE genes from bulk data and thus most distinguish the three lineages. For instance, for the NKT1 lineage, PseudotimeDE's small *p*-values are enriched in the "NKT1 bulk" gene set only, while tradeSeq and Monocle3-DE have small *p*-values enriched in at least two lineage-specific DE gene sets

maturation dataset. The GSEA shows that PseudotimeDE's *p*-values best agree with the lineage-specific DE genes from bulk data and thus most distinguish the three lineages. For example, for the NKT1 lineage, PseudotimeDE's small *p*-values are exclusively enriched in the "NKT1 bulk" gene set, while tradeSeq and Monocle3-DE have small *p*-values enriched in at least two lineage-specific DE gene sets (Fig. 7c). This result confirms that, compared with the DE genes identified by the other two DE methods, the top DE genes identified by PseudotimeDE are more biologically meaningful.

Real data example 5: cell cycle phases

In the fifth application, we compare PseudotimeDE with tradeSeq and Monocle3-DE on a dataset of human induced pluripotent stem cells (iPSCs) measured with cell cycle phases (FUCCI labels) [38]. The original study has reported 101 cyclic genes whose expression levels have large proportions of variance explained (PVE) by cells' FUCCI labels [38]; that is, cells' FUCCI labels are regarded as the predictor, a gene's expression levels in the same cells are regarded as the response, and a PVE is calculated from a nonparametric smoothing fit; hence, the larger the PVE, the better the gene's expression levels can be

predicted by the cell cycle phases. The original study has also developed an R package `peco` to infer cell cycle phases from scRNA-seq data.

In our study, we first construct a benchmark dataset by treating the 101 cyclic genes as true DE genes and using the same genes with expression levels randomly shuffled across cells as the true non-DE genes; hence, our positive and negative sets both contain 101 genes. Then, we apply the R package `peco` to this dataset to infer each cell's cycle phase, which is equivalent to pseudotime; that is, we use `peco` as the pseudotime inference method. Finally, we apply the three DE methods.

Our results show that, for the true non-DE genes, only PseudotimeDE generates valid *p*-values that approximately follow the Uniform[0, 1] distribution (Fig. 8a, & c). For the true DE genes, PseudotimeDE's ($-\log_{10}$ transformed) *p*-values, one per gene, have the highest correlation with these genes' PVE, indicating that PseudotimeDE successfully identifies the top DE genes as those with the strongest cyclic trends (Fig. 8b). PseudotimeDE also yields successful FDR control, the highest AUROC value, and the highest power, among the three DE methods (Fig. 8d–f). Therefore, we conclude that PseudotimeDE

Fig. 8 Application of PseudotimeDE, tradeSeq, and Monocle3-DE to the cell cycle phase dataset. **a** Distributions of non-DE genes' *p*-values by three DE methods with inferred pseudotime. Top: quantile-quantile plots that compare the empirical quantiles of non-DE genes' *p*-values against the expected quantiles of the Uniform[0, 1] distribution. Bottom: histograms of non-DE genes' *p*-values. The *p*-values shown on top of histograms are from the Kolmogorov–Smirnov test under the null hypothesis that the distribution is Uniform[0, 1]. The larger the *p*-value, the more uniform the distribution is. Among the three DE methods, PseudotimeDE's *p*-values follow most closely the expected Uniform[0, 1] distribution. **b** Distributions of DE genes' *p*-values by three DE methods with inferred pseudotime. Top: scatter plots of DE genes' *p*-values against the proportions of variance explained (PVE), which measure the strengths of genes' inferred cyclic trends in the original study [38]. PseudotimeDE's *p*-values ($-\log_{10}$ transformed) have the highest correlation with the PVE, indicating that PseudotimeDE identifies the genes with the strongest cyclic trends as the top DE genes. Bottom: histograms of all genes' *p*-values. Blue and red colors represent the *p*-values of DE genes and non-DE genes (same as in (a) bottom), respectively. PseudotimeDE yields the best separation of the two gene groups' *p*-values. **c** Quantile-quantile plots of the same *p*-values as in **a** on the negative $\log_{10}$ scale. PseudotimeDE returns the best-calibrated *p*-values. **d** FDPs of the three DE methods with the target FDR 0.05 (BH adjusted-$p \leq 0.05$). **e** ROC curves and AUROC values of the three DE methods. PseudotimeDE achieves the highest AUROC. **f** Power of the three DE methods under the FDP = 0.05 cutoff. PseudotimeDE achieves the highest power

outperforms tradeSeq and Monocle3-DE in identifying cell cycle-related genes from this iPSC scRNA-seq dataset.

PseudotimeDE allows users to inspect the uncertainty of inferred cell pseudotime

Besides the identification of DE genes, PseudotimeDE offers functionality for inspecting the uncertainty of pseudotime inference via its intermediate subsampling step. In Figs. 2e, f and 6a, b, PseudotimeDE reveals the uncertainty of inferred cell lineages. Users usually want to fix the lineage topology, e.g., a bifurcation topology, for downstream analysis; however, the topology can vary across subsamples. Hence, we recommend that users check if the inferred topology from the original data can also be inferred from more than half of the subsamples. If not, users may consider using another pseudotime inference method with less uncertainty or adding additional constraints on the inferred topology. Otherwise, the great uncertainty of inferred cell lineage would impair the reliability of downstream analyses.

Next, conditioning on a given lineage topology, PseudotimeDE allows users to visualize the uncertainty of pseudotime within a lineage (Fig. 2a–d), also guiding the choice of pseudotime inference methods in terms of uncertainty.

Computational time

The only feasible way to accommodate all pseudotime inference methods and to account for their uncertainty in DE gene identification is to use subsampling and permutation, the approach taken by PseudotimeDE. However, a common concern of permutation-based methods is that they are computationally intensive. Admittedly, PseudotimeDE is slower than existing non-permutation-based methods, but its computational time is nevertheless acceptable to server users. For example, with 24 cores (Intel "Cascade Lake" CPU), 36 GB RAM and 1000 subsamples, PseudotimeDE takes 3–8 h to analyze each of the first three scRNA-seq datasets in our study. Specifically, the LPS-dendritic cell dataset (4016 genes, 390 cells) takes 3 h, the pancreatic beta cell maturation dataset (6121 genes, 497 cells) takes 3.5 h, and the bone marrow dataset (3004 genes, 2660 cells, two lineages) takes 8 h. The computational time is proportional to the number of genes, the number of lineages, and the number of subsamples. Of course, it is inversely proportional to the number of available cores.

To reduce the computational time of PseudotimeDE, users have two options. First, users may reduce the number of genes to be tested. For instance, lowly expressed genes, such as those with more than 90% of zero counts, are recommended to be filtered out because they are usually of less interest to biologists. Second, users may reduce the number of subsamples. Due to its parametric estimation of the null distribution of the test statistic, PseudotimeDE does not require an enormous number of subsamples. We find that PseudotimeDE with only 100 subsamples generates similar *p*-values to those based on 1000 subsamples (Additional file 1: Fig. S20). If using 100 subsmaples, the computational time is within 0.5 h for each of the first three datasets.

In an undesirable scenario that computational resources are too limited, users have to abandon the consideration of pseudotime uncertainty and treat inferred pseudotime as fixed. Then they do not need the subsampling procedure, and PseudotimeDE will calculate *p*-values from the asymptotic null distribution of the test statistic [39], with short computational time similar to non-permutation-based methods'.

Discussion

We propose a statistical method PseudotimeDE to identify DE genes along inferred cell pseudotime. PseudotimeDE focuses on generating well-calibrated p-values while taking into account the randomness of inferred pseudotime. To achieve these goals, PseudotimeDE first uses subsampling to estimate the uncertainty of pseudotime. Second, PseudotimeDE fits the NB-GAM or ZINB-GAM to both the original dataset and the permuted subsampled datasets to calculate the test statistic and its approximate null values. Next, PseudotimeDE fits a parametric distribution to estimate the approximate null distribution of the test statistic. Finally, PseudotimeDE calculates p-values with a high resolution. PseudotimeDE is flexible to accommodate cell pseudotime inferred in a standard format by any method. Its use of NB-GAM and ZINB-GAM allows it to capture diverse gene expression dynamics and to accommodate undesirable zero inflation in data.

Comprehensive studies on simulated and real data confirm that PseudotimeDE yields better FDR control and higher power than four existing methods (tradeSeq, Monocle3-DE, NBAMSeq, and ImpulseDE2) do. On simulated data, PseudotimeDE generates well-calibrated p-values that follow the uniform distribution under the null hypothesis, while existing methods except Monocle3-DE have p-values violating the uniform assumption. Well-calibrated p-values guarantee the valid FDR control of PseudotimeDE. Moreover, thanks to its use of flexible models NB-GAM and ZINB-GAM, PseudotimeDE has higher power than Monocle3-DE, which uses a more restrictive model GLM and thus has less power. PseudotimeDE also outperforms the other three methods—tradeSeq, NBAMSeq, and ImpulseDE2—that generate ill-calibrated p-values in terms of power. On three real scRNA-seq datasets, the DE genes uniquely identified by PseudotimeDE embrace better biological interpretability revealed by functional analyses, and the p-values of PseudotimeDE lead to more significant GSEA results.

An interesting and open question is what pseudotime inference method works the best with PseudotimeDE. While we observe that PseudotimeDE has higher power with Slingshot than with Monocle3-PI in simulation studies, we realize that the reason may be associated with the simulation design (e.g., the lineage structures), and thus, we cannot draw a conclusion from this observation. Due to the diversity of biological systems and the complexity of pseudotime inference [9], we decide to leave the choice of pseudotime inference methods open to users, and this is the advantage of PseudotimeDE being flexible to accommodate inferred pseudotime by any methods. In practice, we encourage users to try popular pseudotime inference methods and use PseudotimeDE as a downstream step to identify DE genes, so that they can analyze the identification results and decide which pseudotime inference method is more appropriate for their dataset.

The zero inflation, or "dropout" issue, remains perplexing and controversial in the single-cell field [40–44]. The controversy is regarding whether excess zeros that cannot be explained by Poisson or negative binomial distributions are biological meaningful or not. Facing this controversy, we provide two models in PseudotimeDE: NB-GAM and ZINB-GAM, with the former treating excess zeros as biologically meaningful and the latter not. Specifically, the negative binomial distribution in NB-GAM is fitted to all gene expression counts including excess zeros, while the fitting of the negative distribution in ZINB-GAM excludes excess zeros, which ZINB-GAM implicitly treats as non-biological

zeros. PseudotimeDE allows the choice between the two models to be user specified or data driven. From our data analysis, we realize that the choice often requires biological knowledge of the dataset to be analyzed. Specifically, on the LPS-dendritic cell dataset and pancreatic beta cell maturation dataset, we observe that ZINB-GAM leads to power loss: some potential DE genes cannot be identified by ZINB-GAM because zero counts contain useful information (Additional file 1: Figs. S15-S18). Our observation is consistent with another recent study [42], whose authors observed that "zero-inflated models lead to higher false-negative rates than identical non-zero-inflated models." Hence, our real data analysis results are based on NB-GAM. However, realizing the complexity of biological systems and scRNA-seq protocols, we leave the choice between NB-GAM and ZINB-GAM as an option for users of PseudotimeDE, and we encourage users to plot their known DE genes as in Additional file 1: Figs. S15-S18 to decide which of NB-GAM and ZINB-GAM better captures the gene expression dynamics of their interest.

The current implementation of PseudotimeDE is restricted to identifying the DE genes that have expression changes within a cell lineage. While methods including GPfates [45], Monocle2 BEAM [46], and tradeSeq can test whether a gene's expression change is associated with a branching event leading to two lineages, they do not consider the uncertainty of lineage inference. How to account for such topology uncertainty is a challenging open question, as we have seen in Figs. 2f and 6b that the inferred lineage may vary from a bifurcation topology to a trifurcation topology on different subsets of cells. A possible direction is to use the selective inference [47, 48], and we will leave the investigation of this question to future research. Due to this topology uncertainty issue, PseudotimeDE is most suitable for single-cell gene expression data that contain only one cell lineage (including cyclic data) or a small number of well separated cell lineages (e.g., bifurcation and trifurcation). The reason is that these data can maintain stable inferred cell topology after subsampling, an essential requirement of PseudotimeDE. That said, PseudotimeDE is not designed for data with many equivocal cell lineages or a complex cell hierarchy, the data that cannot maintain stable inferred cell topology across subsamples, because for such data, it is difficult to find one-to-one matches between cell lineages inferred from a subsample and those inferred from the original data. Then, a practical solution for such data is to first define a cell lineage of interest and then apply PseudotimeDE to only the cells assigned to that lineage.

There are other open questions to be explored. An important question is: when do we want to identify DE genes along pseudotime? As we have shown in the "Results" section, inferred pseudotime can be highly uncertain. As biologists often sequence cells at multiple physical time points if they want to investigate a biological process, a straightforward analysis is to identify the DE genes that have expression changes across the physical time points. Then, we have two definitions of DE genes: the genes whose expression changes across pseudotime vs. physical time. Understanding which definition is more biologically relevant is an open question. Another question is whether it is possible to integrate pseudotime with physical time to identify biologically relevant DE genes. Answering either question requires a statistical formulation that is directly connected to a biological question.

Another question is how to explore gene-gene correlations along cell pseudotime. Current DE methods only detect marginal gene expression changes but ignore gene-gene

correlations. It remains unclear whether gene-gene correlations are stable or varying along cell pseudotime. Hence, a new statistical method to detect gene-gene correlation changes along inferred pseudotime may offer new biological insights into gene co-expression and regulation at the single-cell resolution.

Methods

PseudotimeDE methodology

Here we describe the methodological detail of PseudotimeDE, a pseudotime-based differential expression testing method. As an overview, PseudotimeDE takes a scRNA-seq count matrix and a pseudotime inference method as input, estimates the uncertainty of pseudotime, performs a differential expression test, and returns a *p*-value of each gene. The core of PseudotimeDE is to obtain a valid null distribution of each DE gene test statistic so that the resulting *p*-value is well-calibrated.

Mathematical notations

We denote by $\mathbf{Y} = (Y_{ij})$ an $n \times m$ gene expression count matrix, whose rows and columns correspond to n cells and m genes, respectively; that is, Y_{ij} is the read count of gene j in cell i. Taking $\mathbf{Y}$ as input, a pseudotime inference method would return a pseudotime vector $\mathbf{T} = (T_1, \ldots, T_i, \ldots, T_n)^{\mathsf{T}}$, where $T_i \in [\,0, 1\,]$ denotes the normalized inferred pseudotime of cell i (i.e., the cells with the smallest and largest pseudotime have $T_i = 0$ and 1, respectively; normalization is used for visualization simplicity). Note that T_i is a random variable due to the random-sampling nature of the n cells and the possible uncertainty introduced by the pseudotime inference method.

Uncertainty estimation

To estimate the uncertainty of pseudotime $\mathbf{T}$, we subsample 80% cells (rows) in $\mathbf{Y}$ for B times. Although there are some theoretical results about the optimal subsample size [49], they do not apply to our problem setting. Hence, we simply choose 80% because it is widely used [50, 51], similar to the popularity of 5-fold cross validation in machine learning [52]. Simulation results also supports that 80% is a reasonable choice, and PseudotimeDE is robust to various subsampling proportions (Additional file 1: Fig. S22; see Additional file 1 for detail). It is worth noting that the bootstrap technique is inapplicable to our problem because it leads to repeated sampling of the same cell, causing issues for some pseudotime inference methods such as Monocle2. If the cells have pre-defined groups (i.e., cell types), we use the stratified sampling by first subsampling 80% cells within each group and then combining these within-group subsamples into one subsample. By default, we set $B = 1000$. For each subsample $\mathbf{Y}^b = (Y_{ij}^b)$, an $n' \times m$ matrix where $n' = \lfloor .8n \rfloor$, we perform pseudotime inference with the same parameters used for the original dataset $\mathbf{Y}$. As a result, we obtain B subsample-based realizations of pseudotime $\mathbf{T}$: $\left\{ \mathbf{T}^1, \cdots, \mathbf{T}^b, \cdots, \mathbf{T}^B \right\}$, where $\mathbf{T}^b \in [\,0, 1\,]^{n'}$, and each cell appears in approximately 80% of these B realizations. Note that we have to apply pseudotime inference to each subsample before permutation to account for pseudotime inference uncertainty; otherwise, if each subsample's pseudotime is just a subsample of all cells' pseudotime, we are essentially treating all cells' pseudotime as fixed, and the uncertainty in pseudotime inference would be ignored. Here is the mathematical explanation. Given that we have n cells with inferred pseudotime as $T_1, \ldots, T_n$, if we use direct subsampling, then in the b-th subsampling,

the subsampled n' cells' pseudotime is just a size-n' subsample of $\{T_1, \ldots, T_n\}$. Instead, in PseudotimeDE, the subsampled n' cells' inferred pseudotime $T_1^b, \ldots, T_{n'}^b$ may be n' values that are not in $T_1, \ldots, T_n$. In other words, the uncertainty in pseudotime inference is reflected in $T_1^b, \ldots, T_{n'}^b$.

PseudotimeDE model

We use the negative binomial–generalized additive model (NB-GAM) as the baseline model to describe the relationship between every gene's expression in a cell and the cell's pseudotime. For gene j ($j = 1, \ldots, m$), its expression Y_{ij} in cell i and the pseudotime T_i of cell i ($i = 1, \ldots, n$) are assumed to follow

$$\begin{cases} Y_{ij} \sim \text{NB}(\mu_{ij}, \phi_j), \\ \log(\mu_{ij}) = \beta_{j0} + f_j(T_i), \end{cases}$$

where $\text{NB}(\mu_{ij}, \phi_j)$ denotes the negative binomial distribution with mean μ_{ij} and dispersion ϕ_j, and $f_j(T_i) = \sum_{k=1}^{K} b_k(T_i)\beta_{jk}$ is a cubic spline function. The number of knots k is predefined as 6 and usually has little effect on results [53]. For gene j, PseudotimeDE fits the NB-GAM to $(Y_{1j}, \ldots, Y_{nj})^\mathsf{T}$ and $\mathbf{T} = (T_1, \ldots, T_n)^\mathsf{T}$ using the R package mgcv (version 1.8.31), which estimates model parameters by penalized-restricted maximum likelihood estimation.

To account for excess zeros in scRNA-seq data that may not be explained by the NB-GAM, we introduce a hidden variable Z_{ij} to indicate the "dropout" event of gene j in cell i, and the resulting model is called the zero-inflated negative binomial–generalized additive model (ZINB-GAM):

$$\begin{cases} Z_{ij} \sim \text{Ber}(p_{ij}), \\ Y_{ij}|Z_{ij} \sim Z_{ij} \cdot \text{NB}(\mu_{ij}, \phi_j) + (1 - Z_{ij}) \cdot 0, \\ \log(\mu_{ij}) = \beta_{j0} + f_j(T_i), \\ \text{logit}(p_{ij}) = \alpha_{j0} + \alpha_{j1}\log(\mu_{ij}). \end{cases}$$

For gene j, PseudotimeDE fits the ZINB-GAM to $(Y_{1j}, \ldots, Y_{nj})^\mathsf{T}$ and $\mathbf{T} = (T_1, \ldots, T_n)^\mathsf{T}$ using the expectation-maximization (EM) algorithm, which is partially based on R package zigam [54]. To use PseudotimeDE, users can specify whether to use the ZINB-GAM or NB-GAM. If users do not provide a specification, PseudotimeDE will automatically choose between the two models for each gene by the Akaike information criterion (AIC). By default, PseudotimeDE uses NB-GAM unless the AIC of ZINB-GAM exceeds the AIC of NB-GAM by at least 10, a threshold suggested by [55].

Statistical test and p-value calculation

To test if gene j is DE along cell pseudotime, PseudotimeDE defines the null and alternative hypotheses as

$$H_0 : f_j(\cdot) = 0 \quad \text{vs.} \quad H_1 : f_j(\cdot) \neq 0$$

We denote the estimate of $\left(f_j(T_1), \ldots, f_j(T_n)\right)^\mathsf{T}$ by $\hat{\boldsymbol{f}}_j$, whose estimated covariance matrix (of dimensions $n \times n$) is denoted by $\widehat{\mathbf{V}}_{f_j}$. Then, the test statistic is

$$S_j = \hat{\boldsymbol{f}}_j^\mathsf{T} \widehat{\mathbf{V}}_{f_j}^{r-} \hat{\boldsymbol{f}}_j,$$

where $\widehat{\mathbf{V}}_{f_j}^{r-}$ is the rank-r pseudoinverse of $\widehat{\mathbf{V}}_{f_j}$, where r is determined in the way described in [39]. When the T_i's are fixed, the asymptotic null distribution of S_j is described in [39], and the p-value can be calculated by the R package mgcv.

A key novelty of PseudotimeDE is its accounting for the uncertainty of inferred pseudotime. When the T_i's are random, the asymptotic null distribution of S_j given that T_i's are fixed [39] and the p-value calculation in the R package mgcv no longer apply. To address this issue and estimate the null distribution, PseudotimeDE uses the following permutation procedure: (1) PseudotimeDE randomly permutes each subsample-based realization $\mathbf{T}^b = (T_1^b, \ldots, T_{n'}^b)^\mathsf{T}$ into $\mathbf{T}^{*b} = (T_1^{*b}, \ldots, T_{n'}^{*b})^\mathsf{T}$; (2) PseudotimeDE fits the above model to $(Y_{1j}^b, \ldots, Y_{n'j}^b)^\mathsf{T}$ and $\mathbf{T}^{*b}$ and calculates the test statistic S_j's value as s_j^b using the R package mgcv; and (3) PseudotimeDE performs (1) and (2) for $b = 1, \ldots, B$ and collects the resulting $\{s_j^1, \ldots, s_j^B\}$ as the null values of the test statistic S_j.

Then, PseudotimeDE estimates the null distribution of S_j in two ways. Based on the estimated null distribution in either way and the observed test statistic value s_j, which is calculated from the original dataset by the R package mgcv, PseudotimeDE calculates a p-value for gene j.

1. **Empirical estimate**. PseudotimeDE uses the empirical distribution of $\{s_j^1, \ldots, s_j^B\}$ as the estimated null distribution. Following the suggestion in [56], PseudotimeDE calculates the p-value of gene j as

$$p_j^{\text{emp}} = \frac{\sum_{b=1}^B \mathbb{I}(s_j^b \geq s_j) + 1}{B + 1},$$

where $\mathbb{I}(\cdot)$ is the indicator function. We refer to this p-value as the "empirical p-value."

2. **Parametric estimate**. The resolution of p_j^{emp} depends on the number of permutations B, because the smallest value p_j^{emp} may take is $1/(B + 1)$. Although users often cannot afford a too large B due to limited computational resources, they still desire a high resolution of p-values to control the FDR to a small value (e.g., 5%) when the number of tests (i.e., the number of genes in DE gene identification) is large. To increase the resolution of p-values, PseudotimeDE fits a parametric distribution to $\{s_j^1, \ldots, s_j^B\}$ and uses the fitted distribution as the estimated null distribution. Driven by the empirical distribution of $\{s_j^1, \ldots, s_j^B\}$, PseudotimeDE considers two parametric distributions: (1) a gamma distribution $\Gamma(\alpha, \beta)$ with $\alpha, \beta > 0$ and (2) a two-component gamma mixture model $\gamma \Gamma(\alpha_1, \beta_1) + (1 - \gamma)\Gamma(\alpha_2, \beta_2)$ with $0 < \gamma < 1$ and $\alpha_1, \beta_1, \alpha_2, \beta_2 > 0$. After fitting both distributions to $\{s_j^1, \ldots, s_j^B\}$ using the maximum likelihood estimation (gamma distribution fit by the R package fitdistrplus (version 1.0.14) [57] and gamma mixture model fit by the R package mixtools (version 5.4.5) [58]), PseudotimeDE chooses between the two fitted distributions by performing the likelihood ratio test (LRT) with 3 degrees of freedom (i.e., difference in the numbers of parameters between the two distributions). If the LRT p-value is less or equal than 0.01, PseudotimeDE uses the fitted two-component gamma mixture model as the parametric estimate of the null distribution of S_j; otherwise, PseudotimeDE uses the fitted gamma distribution. The Anderson-Darling goodness-of-fit test verifies that such a parametric approach fits the empirical distributions well (Additional file 1: Fig. S21). Denoting the cumulative distribution

function of the parametrically estimated null distribution by $\hat{F}_j(\cdot)$, PseudotimeDE calculates the p-value of gene j as

$$p_j^{\text{param}} = 1 - \hat{F}_j(s_j),$$

where is referred to as the "parametric p-value."

PseudotimeDE outputs both p_j^{emp} and p_j^{param} for gene j, $j = 1, \ldots, m$. Empirical evidence shows that parametric p-values agree with empirical p-values well across the $[0, 1]$ interval (Additional file 1: Fig. S19). All the findings in the "Results" section are based on $p_1^{\text{param}}, \ldots, p_m^{\text{param}}$ due to their higher resolution.

Pseudotime inference methods

We apply two state-of-the-art methods, Slingshot and Monocle3-PI, to inferring the cell pseudotime of each dataset. For single-lineage data, we specify the start cluster in Slingshot and the start node in Monocle3-PI. For bifurcation/trifurcation data, we specify the start cluster/node and the end clusters/nodes in Slingshot/Monocle3-PI. By default, the dimensionality reduction methods used for pseudotime inference are PCA and UMAP for Slingshot and Monocle3-PI, respectively. The R Bioconductor package `slingshot` (version 1.4.0) and the R package `monocle3` (version 0.2.0) are used.

DE analysis methods

We compare PseudotimeDE with four existing methods for identifying DE genes along pseudotime/time-course from scRNA-seq data (tradeSeq and Monocle3-DE) or bulk RNA-seq data (ImpulseDE2 and NBAMSeq). All these methods take a count matrix **Y** and a pseudotime vector **T** as input, and they return a p-value for each gene. For tradeSeq, we use the functions `fitGAM` and `associationTest` (https://statomics.github.io/tradeSeq/articles/tradeSeq.html). The number of knots parameter K in trade-Seq is chosen by 100 random genes based on the tradeSeq vignette. For Monocle3-DE, we use the function `fit_models` (https://cole-trapnell-lab.github.io/monocle3/docs/differential/). Since ImpulseDE2 cannot be applied to scRNA-seq data directly, we follow the modified implementation of ImpulseDE2 in the tradeSeq paper (https://github.com/statOmics/tradeSeqPaper). The R Bioconductor packages `tradeSeq` (version 1.3.15), `monocle3` (version 0.2.0), `ImpulseDE2` (version 1.10.0), and `NBAMSeq` (version 1.10.0) are used.

Functional (gene ontology and gene-set enrichment) analyses

We use the R package `topGO` (version 2.38.1) [59] to perform the gene-ontology (GO) enrichment analysis on identified DE genes. We use the R package `clusterProfiler` (version 3.14.3) [60] to perform the gene-set enrichment analysis (GSEA) on ranked gene lists, where genes in each list are ranked by their ranking sores defined as $-\log_{10}$ transformed p-values (the gene with the smallest p-value is ranked the top); p-values that are exactly zeros are replaced by one-tenth of the smallest non-zero p-value. If unspecified, the GO terms are "biological process (BP)" terms.

Simulation study

We use the R package `dyntoy` (0.9.9) to generate single-lineage data and bifurcation data. For single-lineage data, we generate three datasets with increasing dispersion levels (low

dispersion, medium dispersion, and high dispersion). Each single-lineage dataset consists of 500 cells and 5000 genes (with 20% as DE genes). For bifurcation data, we use the medium dispersion level. The bifurcation dataset consists of 750 cells and 5000 genes (with 20% as DE genes).

Case studies

LPS-dendritic cell dataset: this Smart-seq dataset contains primary mouse dendritic cells (DCs) stimulated with lipopolysaccharide (LPS) [31], available at Gene Expression Omnibus (GEO) under accession ID GSE45719. In our analysis, we use the cells from 1h, 2h, 4h, and 6h in the pre-processed data from the study that benchmarked pseudotime inference methods [9]. After the genes with > 90% zeros are removed, the final dataset consists of 4016 genes and 390 cells, which are expected to be in a single lineage. When applying tradeSeq, we use the recommended ZINB-WaVE [61] + tradeSeq procedure to account for potential zero-inflation. The R Bioconductor package `zinbwave` (version 1.8.0) is used.

Pancreatic beta cell maturation dataset: this Smart-seq2 dataset measures the maturation process of mouse pancreatic beta cells [33], available at GEO under accession ID GSE87375. We use the cells from cell type "beta" in the pre-processed data from the study that benchmarked pseudotime inference methods [9]. After the genes with > 90% zeros are removed, the final dataset consists of 6121 genes and 497 cells, which are expected to be in a single lineage. When applying tradeSeq, we use the recommended ZINB-WaVE + tradeSeq procedure to account for potential zero-inflation. The R Bioconductor package `zinbwave` (version 1.8.0) is used.

Mouse bone marrow dataset: this MARS-seq dataset contains myeloid progenitors in mouse bone marrow [36], available at GEO under accession ID GSE72859. We use the pre-processed data provided by the tradeSeq vignette. After the genes with > 90% zeros are removed, the final dataset consists of 3004 genes and 2660 cells. We follow the procedure of combining UMAP and Slingshot to infer pseudotime as described in tradeSeq paper [16]

Natural killer T cell dataset: this Smart-seq2 dataset measures four natural killer T cell (NKT cell) subtypes in mouse [37], available at GEO under accession ID GSE74597. We use the pre-processed data from the study that benchmarked pseudotime inference methods [9]. After the genes with > 90% zeros are removed, the final dataset consists of 5270 genes and 197 cells, which are expected to have three lineages. We use PCA + Slingshot to infer the pseudotime. When applying tradeSeq, we use the recommended ZINB-WaVE + tradeSeq procedure to account for potential zero-inflation. The R Bioconductor package `zinbwave` (version 1.8.0) is used.

Cell cycle phase dataset: this Fluidigm protocol dataset measures human induced pluripotent stem cells (iPSCs) [38]. The iPSCs were FUCCI-expressing so that their cell cycle phases were tracked. The authors also developed an R package `peco` for predicting cell cycle phases from single-cell gene expression data. We use the example dataset provided by `peco`, which consists of 101 known cell cycle-related genes (DE genes). To construct null cases, we randomly shuffle the 101 DE genes' expression levels across cells to create 101 non-DE genes. The final dataset consists of 202 genes and 888 cells. We use the R package `peco` (version 1.1.21) to infer cell cycle phases.

Supplementary Information

The online version contains supplementary material available at https://doi.org/10.1186/s13059-021-02341-y.

Additional file 1: Supplementary materials. It includes all supplementary text and figures.

Additional file 2: Supplementary table 1. It includes enrichment analysis results of LPS-dendritic cell dataset.

Additional file 3: Supplementary table 2. It includes enrichment analysis results of pancreatic beta cell maturation dataset.

Additional file 4: Supplementary table 3. It includes enrichment analysis results of mouse bone marrow dataset.

Additional file 5: Review history.

Peer review information
Barbara Cheifet was the primary editor of this article and managed its editorial process and peer review in collaboration with the rest of the editorial team.

Review history
The review history is available as Additional file 5.

Authors' contributions
D.S. and J.J.L. designed the research. D.S. conducted the research and wrote the computer code. J.J.L. supervised the project. D.S. and J.J.L. discussed the results and wrote the manuscript. The authors read and approved the final manuscript.

Availability of data and materials
The R package `PseudotimeDE` is available at https://github.com/SONGDONGYUAN1994/PseudotimeDE [62] under the MIT license. The source code and data for reproducing the results are available at http://doi.org/10.5281/zenodo.4663580 [63].

Declarations

Ethics approval and consent to participate
None.

Consent for publication
Not applicable for this study.

Competing interests
The authors declare that they have no competing interests.

Author details
[1] Bioinformatics Interdepartmental Ph.D. Program, University of California, Los Angeles, CA 90095-7246, USA. [2] Department of Statistics, University of California, Los Angeles, CA 90095-1554, USA. [3] Department of Human Genetics, University of California, Los Angeles, CA 90095-7088, USA. [4] Department of Computational Medicine, University of California, Los Angeles, CA 90095-1766, USA. [5] Department of Biostatistics, University of California, Los Angeles, CA 90095-1772, USA.

References
1. Haque A, Engel J, Teichmann SA, Lönnberg T. A practical guide to single-cell RNA-sequencing for biomedical research and clinical applications. Genome Med. 2017;9(1):1–12.
2. Kiselev VY, Andrews TS, Hemberg M. Challenges in unsupervised clustering of single-cell RNA-seq data. Nat Rev Genet. 2019;20(5):273–82.
3. Papalexi E, Satija R. Single-cell RNA sequencing to explore immune cell heterogeneity. Nat Rev Immunol. 2018;18(1):35.
4. Tritschler S, Büttner M, Fischer DS, Lange M, Bergen V, Lickert H, Theis FJ. Concepts and limitations for learning developmental trajectories from single cell genomics. Development. 2019;146(12):dev170506.
5. Croft AP, Campos J, Jansen K, Turner JD, Marshall J, Attar M, Savary L, Wehmeyer C, Naylor AJ, Kemble S, et al. Distinct fibroblast subsets drive inflammation and damage in arthritis. Nature. 2019;570(7760):246–51.

6.   Vento-Tormo R, Efremova M, Botting RA, Turco MY, Vento-Tormo M, Meyer KB, Park J-E, Stephenson E, Polański K, Goncalves A, et al. Single-cell reconstruction of the early maternal–fetal interface in humans. Nature. 2018;563(7731):347–53.

7.   Park J-E, Botting RA, Conde CD, Popescu D-M, Lavaert M, Kunz DJ, Goh I, Stephenson E, Ragazzini R, Tuck E, et al. A cell atlas of human thymic development defines T cell repertoire formation. Science. 2020;367(6480):eaay3224.

8.   Trapnell C, Cacchiarelli D, Grimsby J, Pokharel P, Li S, Morse M, Lennon NJ, Livak KJ, Mikkelsen TS, Rinn JL. The dynamics and regulators of cell fate decisions are revealed by pseudotemporal ordering of single cells. Nat Biotechnol. 2014;32(4):381.

9.   Saelens W, Cannoodt R, Todorov H, Saeys Y. A comparison of single-cell trajectory inference methods. Nat Biotechnol. 2019;37(5):547–54.

10.   Ji Z, Ji H. TSCAN: Pseudo-time reconstruction and evaluation in single-cell RNA-seq analysis. Nucleic Acids Res. 2016;44(13):e117.

11.   Street K, Risso D, Fletcher RB, Das D, Ngai J, Yosef N, Purdom E, Dudoit S. Slingshot: cell lineage and pseudotime inference for single-cell transcriptomics. BMC Genomics. 2018;19(1):477.

12.   Qiu X, Mao Q, Tang Y, Wang L, Chawla R, Pliner HA, Trapnell C. Reversed graph embedding resolves complex single-cell trajectories. Nat Methods. 2017;14(10):979.

13.   Hastie TJ, Tibshirani RJ, Vol. 43. Generalized additive models: CRC press; 1990.

14.   Wood SN. mgcv: GAMs and generalized ridge regression for R. R News. 2001;1(2):20–5.

15.   Yee TW. The VGAM package. R News. 2008;8(2):28–39.

16.   Van den Berge K, De Bezieux HR, Street K, Saelens W, Cannoodt R, Saeys Y, Dudoit S, Clement L. Trajectory-based differential expression analysis for single-cell sequencing data. Nat Commun. 2020;11(1):1–13.

17.   Cao J, Spielmann M, Qiu X, Huang X, Ibrahim DM, Hill AJ, Zhang F, Mundlos S, Christiansen L, Steemers FJ, et al. The single-cell transcriptional landscape of mammalian organogenesis. Nature. 2019;566(7745):496–502.

18.   Hao N, O'shea EK. Signal-dependent dynamics of transcription factor translocation controls gene expression. Nat Struct Mol Biol. 2012;19(1):31.

19.   Ren X, Kuan P-F. Negative binomial additive model for RNA-Seq data analysis. BMC Bioinformatics. 2020;21:1–15.

20.   Fischer DS, Theis FJ, Yosef N. Impulse model-based differential expression analysis of time course sequencing data. Nucleic Acids Res. 2018;46(20):e119.

21.   Love MI, Huber W, Anders S. Moderated estimation of fold change and dispersion for RNA-seq data with DESeq2. Genome Biol. 2014;15(12):550.

22.   Spies D, Renz PF, Beyer TA, Ciaudo C. Comparative analysis of differential gene expression tools for RNA sequencing time course data. Brief Bioinform. 2019;20(1):288–98.

23.   Kharchenko PV, Silberstein L, Scadden DT. Bayesian approach to single-cell differential expression analysis. Nat Methods. 2014;11(7):740–2.

24.   Finak G, McDavid A, Yajima M, Deng J, Gersuk V, Shalek AK, Slichter CK, Miller HW, McElrath MJ, Prlic M, et al. MAST: a flexible statistical framework for assessing transcriptional changes and characterizing heterogeneity in single-cell RNA sequencing data. Genome Biol. 2015;16(1):1–13.

25.   Vu TN, Wills QF, Kalari KR, Niu N, Wang L, Rantalainen M, Pawitan Y. Beta-Poisson model for single-cell RNA-seq data analyses. Bioinformatics. 2016;32(14):2128–35.

26.   Korthauer KD, Chu L-F, Newton MA, Li Y, Thomson J, Stewart R, Kendziorski C. A statistical approach for identifying differential distributions in single-cell RNA-seq experiments. Genome Biol. 2016;17(1):222.

27.   Soneson C, Robinson MD. Bias, robustness and scalability in single-cell differential expression analysis. Nat Methods. 2018;15(4):255.

28.   Campbell KR, Yau C. Order under uncertainty: robust differential expression analysis using probabilistic models for pseudotime inference. PLoS Comput Biol. 2016;12(11):e1005212.

29.   Strauß ME, Reid JE, Wernisch L. GPseudoRank: a permutation sampler for single cell orderings. Bioinformatics. 2019;35(4):611–8.

30.   Giecold G, Marco E, Garcia SP, Trippa L, Yuan G-C. Robust lineage reconstruction from high-dimensional single-cell data. Nucleic Acids Res. 2016;44(14):e122.

31.   Shalek AK, Satija R, Shuga J, Trombetta JJ, Gennert D, Lu D, Chen P, Gertner RS, Gaublomme JT, Yosef N, et al. Single-cell RNA-seq reveals dynamic paracrine control of cellular variation. Nature. 2014;510(7505):363–9.

32.   Subramanian A, Tamayo P, Mootha VK, Mukherjee S, Ebert BL, Gillette MA, Paulovich A, Pomeroy SL, Golub TR, Lander ES, et al. Gene set enrichment analysis: a knowledge-based approach for interpreting genome-wide expression profiles. Proc Natl Acad Sci. 2005;102(43):15545–50.

33.   Qiu W-L, Zhang Y-W, Feng Y, Li L-C, Yang L, Xu C-R. Deciphering pancreatic islet β cell and α cell maturation pathways and characteristic features at the single-cell level. Cell Metab. 2017;25(5):1194–205.

34.   Apelqvist Å, Li H, Sommer L, Beatus P, Anderson DJ, Honjo T, de Angelis MH, Lendahl U, Edlund H. Notch signalling controls pancreatic cell differentiation. Nature. 1999;400(6747):877–81.

35.   Lawson R, Maret W, Hogstrand C. Expression of the ZIP/SLC39A transporters in β-cells: a systematic review and integration of multiple datasets. BMC Genomics. 2017;18(1):719.

36.   Paul F, Arkin Y, Giladi A, Jaitin DA, Kenigsberg E, Keren-Shaul H, Winter D, Lara-Astiaso D, Gury M, Weiner A, et al. Transcriptional heterogeneity and lineage commitment in myeloid progenitors. Cell. 2015;163(7):1663–77.

37.   Engel I, Seumois G, Chavez L, Samaniego-Castruita D, White B, Chawla A, Mock D, Vijayanand P, Kronenberg M. Innate-like functions of natural killer T cell subsets result from highly divergent gene programs. Nat Immunol. 2016;17(6):728–39.

38.   Hsiao CJ, Tung P, Blischak JD, Burnett JE, Barr KA, Dey KK, Stephens M, Gilad Y. Characterizing and inferring quantitative cell cycle phase in single-cell RNA-seq data analysis. Genome Res. 2020;30(4):611–21.

39.   Wood SN. On p-values for smooth components of an extended generalized additive model. Biometrika. 2013;100(1):221–8.

40.   Hicks SC, Townes FW, Teng M, Irizarry RA. Missing data and technical variability in single-cell RNA-sequencing experiments. Biostatistics. 2018;19(4):562–78.

41. Svensson V. Droplet scRNA-seq is not zero-inflated. Nat Biotechnol. 2020;38(2):147–50.
42. Silverman JD, Roche K, Mukherjee S, David LA. Naught all zeros in sequence count data are the same. Comput Struct Biotechnol J. 2020;18:2789.
43. Choi K, Chen Y, Skelly DA, Churchill GA. Bayesian model selection reveals biological origins of zero inflation in single-cell transcriptomics. Genome Biol. 2020;21(1):1–16.
44. Kim TH, Zhou X, Chen M. Demystifying "drop-outs" in single-cell UMI data. Genome Biol. 2020;21(1):1–19.
45. Lönnberg T, Svensson V, James KR, Fernandez-Ruiz D, Sebina I, Montandon R, Soon MSF, Fogg LG, Nair AS, Liligeto U, et al. Single-cell RNA-seq and computational analysis using temporal mixture modelling resolves Th1/Tfh fate bifurcation in malaria. Sci Immunol. 2017;2(9):eaal2192.
46. Qiu X, Hill A, Packer J, Lin D, Ma Y-A, Trapnell C. Single-cell mRNA quantification and differential analysis with Census. Nat Methods. 2017;14(3):309–15.
47. Berk R, Brown L, Buja A, Zhang K, Zhao L, et al. Valid post-selection inference. Ann Stat. 2013;41(2):802–37.
48. Lee JD, Sun DL, Sun Y, Taylor JE, et al. Exact post-selection inference, with application to the lasso. Ann Stat. 2016;44(3):907–27.
49. Politis DN, Romano JP, Wolf M. Subsampling: Springer Science & Business Media; 1999.
50. Tseng GC, Wong WH. Tight clustering: a resampling-based approach for identifying stable and tight patterns in data. Biometrics. 2005;61(1):10–6.
51. Sun YE, Zhou HJ, Li JJ. Bipartite Tight Spectral Clustering (BiTSC) Algorithm for Identifying Conserved Gene Co-clusters in Two Species. Bioinformatics. 2020;btaa741. https://doi.org/10.1093/bioinformatics/btaa741.
52. Hastie T, Tibshirani R, Friedman J. The elements of statistical learning: data mining, inference, and prediction: Springer Science & Business Media; 2009.
53. Wood SN. Generalized additive models: an introduction with R: CRC press; 2017.
54. Wotherspoon S, Burch P. zigam: EM implementation of zero-inflated GAMs; 2016. https://github.com/AustralianAntarcticDataCentre/zigam.
55. Burnham KP, Anderson DR. Multimodel inference: understanding AIC and BIC in model selection. Sociol Methods Res. 2004;33(2):261–304.
56. Phipson B, Smyth GK. Permutation P-values Should Never Be Zero: Calculating Exact P-values When Permutations Are Randomly Drawn. Stat Appl Genet Mol Biol. 2021;9(1). Article 39.
57. Delignette-Muller ML, Dutang C. fitdistrplus: An R package for fitting distributions. J Stat Softw. 2015;64(4):1–34. http://www.jstatsoft.org/v64/i04/.
58. Benaglia T, Chauveau D, Hunter D, Young D. mixtools: An R package for analyzing finite mixture models. J Stat Softw. 2009;32(6):1–29. http://www.jstatsoft.org/v32/i06/.
59. Alexa A, Rahnenführer J, Vol. 27. Gene set enrichment analysis with topGO; 2009, pp. 1–26.
60. Yu G, Wang L-G, Han Y, He Q-Y. clusterProfiler: an R package for comparing biological themes among gene clusters. OMICS J Integr Biol. 2012;16(5):284–7. https://doi.org/10.1089/omi.2011.0118.
61. Risso D, Perraudeau F, Gribkova S, Dudoit S, Vert J-P. A general and flexible method for signal extraction from single-cell RNA-seq data. Nat Commun. 2018;9(1):1–17.
62. Song D. PseudotimeDE: Inference of differential gene expression along cell pseudotime with well-calibrated p-values from single-cell RNA sequencing data. Github. 2021. https://github.com/SONGDONGYUAN1994/PseudotimeDE.
63. Song D, Li JJ. PseudotimeDE: inference of differential gene expression along cell pseudotime with well-calibrated p-values from single-cell RNA sequencing data. Zenodo. 2021. https://doi.org/10.5281/zenodo.4663580.

Publisher's Note

Springer Nature remains neutral with regard to jurisdictional claims in published maps and institutional affiliations.